Available online at www.sciencedirect.com
SCIENCE DIRECT
Polymer 46 (2005) 6360–6368
polymer
www.elsevier.com/locate/polymer

Analysis of polymer blend morphologies from transmission electron micrographs

Laurent Corté*, Ludwik Leibler

Matière Molle et Chimie, Ecole Supérieure de Physique Chimie Industrielle (UMR ESPCI-CNRS 7167), 10 rue Vauquelin, 75231 Paris Cedex 05, France

Received 18 April 2005; received in revised form 23 May 2005; accepted 24 May 2005
Available online 22 June 2005

Abstract

Thermomechanical properties of polymer blends seem to depend on their morphology on microscales and in particular on the size of the dispersed phase particles and/or their distances (ligament thickness). Precise characterization of morphologies by few simple geometrical parameters is often a quite delicate task, in particular because of the strong polydispersity of these systems. We present here a simple method based on image analysis of transmission electron micrographs (TEM) to estimate both distributions in particle size and ligament thickness. We first reconstruct three-dimensional distributions in particle size from two-dimensional measurements and show in particular that corrections from section thickness become significant when thickness is comparable to particle size. Knowing the distribution in particle size, we extend the model initially proposed by Wu to estimate the distribution in ligament thickness. This method provides a more detailed relation between the distribution in particle size and the distribution in ligament thickness. Advantages and limitations of the method are illustrated by practical examples on polyamide-12 systems filled with various particle dispersions.

Keywords: Polymer blends; Image analysis; Transmission electron microscopy

1. Introduction

Polymer blending offers an extraordinary rich range of new materials with enhanced characteristics regarding optical, chemical or mechanical performances [1,2]. For instance, the mechanical properties of a given polymer can be greatly modified—either improved or worsened—by incorporating particles of a second minority phase. Most often, the quality of the morphology (size, continuity, homogeneity, orientation…) is crucial for the final performances of these heterogeneous materials. In particular, Wu showed that the impact resistance of semi-crystalline polymers toughened with rubber particles is intimately related to the average ligament thickness, L_n, which is defined as the average surface-to-surface distance between neighbored particles [3]. In given impact conditions, a toughened system exhibits a ductile behavior when L_n is lower than some critical value while it gets brittle for larger values of L_n. Recent studies suggest that toughening efficiency also depends on several other parameters such as particle size [4], crystalline orientation [5] or more generally crystalline organization of the matrix [6] which are often strongly processing-dependent. Still, the quantitative characterization of the blend morphologies is of paramount importance. For example, Fig. 1(a) and (b) shows micrographs of two distinct samples of polyamide-12 toughened by blending with the same copolymer. The impact toughness of these two samples are very different. Indeed, their notched Charpy impact toughness at 25 °C are 100 and 80 kJ/m^2, respectively. Are the morphologies as different as impact experiments could suggest? Qualitatively, they look very similar but can one be certain? In fact, micrograph b is an image of the injected sample shown on image a after a thermal treatment (quiescent melting and recrystallization) which in principle does not alter the dispersion morphology. On the other hand, the dispersion shown on Fig. 1(c) looks much denser than those on Fig. 1(a) or (b). One could expect very different mechanical properties. Yet, it is the same sample as in Fig. 1(a) but the ultrathin section observed under TEM is about twice thicker. Hence, quantitative techniques which characterize

* Corresponding author. Tel.: +33 1 40 79 51 22; fax: +33 1 40 79 51 17.
E-mail addresses: laurent.corte@espci.fr (L. Corté), ludwik.leibler@espci.fr (L. Leibler).

0032-3861/$ - see front matter © 2005 Elsevier Ltd. All rights reserved.
doi:10.1016/j.polymer.2005.05.109

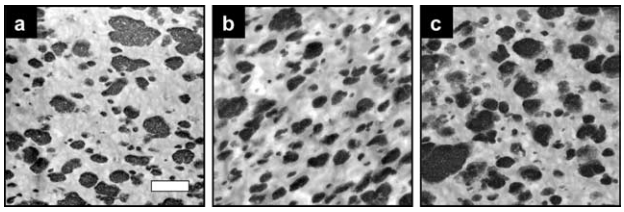

Fig. 1. Transmission electron micrographs of polyamide-12 toughened with 30% SBM particles (a) morphology of an injected sample (b) same sample as in *a* after a thermal treatment where the polyamide matrix was melted and recrystallized under quiescent conditions (c) same sample as in *a* but observation is done on a thicker ultrathin section.

particle dispersions are essential tools to understand how impact performances depend on the blend morphology and how they can be controlled in terms of compounding and processing.

Here, we present a fairly simple method based on image analysis of transmission electron micrographs to determine both distributions of particle sizes and ligament thicknesses. Image analysis is traditionally performed with scanning electron microscopy (SEM). In the present study, we use transmission electron microscopy (TEM) which provides additional information at finer scales about the possible nanostructure of the particles and/or the crystalline organization of the matrix. Unlike SEM which shows cross-sections of the bulk morphology, TEM shows a 2D projection of a thin section of about 50–100 nm thick. In order reconstruct the true 3D distribution in particle size, we consider some specific features of the TEM technique as illustrated in Fig. 2. A 'cross-section' effect, which also exists with SEM, arises from the fact that the observed micrograph is a 2D section of randomly cut particles. As a result, the apparent diameter of a particle on the image is smaller than its real diameter as soon as the particle is not cut through its center. This is the case of particles 1 and 3 in Fig. 2. Such effect implies that raw measurements overestimate the fraction of small particles. On the other hand, a 'projection' effect, which is more specific to transmission microscopy, comes from the finite thickness of the thin section. All the particles which center is inside the thin film appear on the image with their real diameter as shown in Fig. 2 for particle 2. Hence, this latter effect can

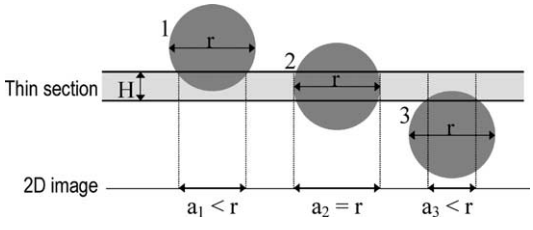

Fig. 2. Transmission microscopy shows a two-dimensional projection of a thin section. Particles 1, 2 and 3 have the same diameter, *r*. The center of particles 1 and 3 are above and below the thin section, respectively. Their apparent diameters a_1 and a_3 are smaller than their real diameter *r* (cross section effect). The center of particle 2 is inside the thin section. It appears on the image with its real diameter (projection effect).

counterbalance the former cross-section effect. We correct both effects using a Schwartz-Saltikov algorithm for sections of finite thickness [7,8].

Unlike particle size and concentration which are rather well-controlled and measured, the ligament thickness is difficult to measure in a straightforward way. This difficulty is mostly due to the ambiguous definition of 'neighbored particles' and to the reconstruction of true three-dimensional (3D) distributions from two-dimensional (2D) measurements. A first model proposed by Wu infers the average ligament thickness given the distribution in particle size [3]. Particles are assumed to be spherical, of same diameter and regularly packed on a periodic lattice. The average ligament thickness, L_n, is then estimated as follows:

$$L_n = d_n\left(C\left(\frac{\pi}{6\Phi}\right)^{1/3} - 1\right) \quad (1)$$

where d_n is the number average particle diameter, Φ the filler volume fraction and C a constant characterizing the lattice. This initial formula has later been modified in several subsequent studies, in particular to consider cases with a distribution in particle sizes [9,10]. However, the proposed expression only gives an average value of the ligament thickness while the shape of the whole distribution may have a significant role. For instance, the ability to initiate and propagate plastic deformation may be more sensitive to the fraction of thinner ligaments. Recently, Sigalov et al. developed an alternative and rigorous method which measures directly on the image the 2D distribution in ligament thickness [11]. The authors have captured significant effects of packing on the distribution in ligament thickness. In particular, they found that the ligament thickness distribution evolves during processing due to changes in particle packing alone. Such phenomenon could not be measured with the previous indirect method which assumes a lattice-like packing of particles.

The intermediate method proposed here extends the indirect model of Wu to estimate the whole 3D distribution in ligament thickness. Once the 3D distribution in particle size has been determined, we deduce the corresponding distribution in ligament thickness assuming that particles are spherical and arranged on a periodic lattice. These calculations provide additional details about the morphology and in particular, an estimation of the standard deviation in ligament thickness. The paper is organized as follows. The algorithm to correct TEM measurements and reconstruct the 3D distribution in particle size is given in a first part. A second part presents the estimation of the distribution in ligament thickness. Practical cases on polyamide-12 systems filled with copolymer particles illustrate the interests and limitations of each step. In particular, we use these examples to discuss the accuracy of the method and the restrictions induced by the lattice-like packing assumption.

2. Experimental

2.1. Materials

The method presented here has been applied to toughened polyamide-12 systems provided by Arkema. Here, the impact fillers are a polystyrene-*block*-polybutadiene-*block*-poly(methyl methacrylate) triblock copolymer (SBM) and a polystyrene-*block*-polybutadiene-block-poly[(methyl methacrylate)-*stat*-(*tert*-butyl methacrylate)] triblock copolymer (SB(MT)) which can react with the polyamide matrix. The synthesis of reactive SB(MT) block copolymers is described in a previous study [12]. Blending was achieved by extruding together the filler and the semicrystalline matrix. Different particle sizes and ligament thicknesses were obtained by varying the reactivity between the filler and the matrix as well as the processing conditions. More details about the preparation, morphology and performances of these systems can be found in other studies [6,13].

2.2. Characterization

Particle dispersions were characterized by transmission electron microscopy (TEM) using stained ultrathin sections. Ultrathin films of about 60 nm thick were cut by ultramicrotomy on a Leica Ultracut apparatus with a diamond knife at −100 °C. Osmium tetroxide (OsO_4) vapor was used to selectively stain SBM particles. Experiments were carried out with a JEOL 100CX electron microscope at an acceleration voltage of 80 kV.

2.3. Image analysis

For each blend, particle size distribution was obtained by image analysis with the ImageJ software [14] on 200–800 particles and over several tens of μm^2.

3. Results and discussion

3.1. Distribution in particle size

3.1.1. Data collection

Most image analysis softwares only treat binarized images: black particles for instance, distributed in a white matrix. Such images can be difficult to obtain because accurate binarization requires a clear initial image with good contrast between matrix and particles. Here, we only focus on the data treatment once the image has been binarized. As an example, a TEM micrograph of toughened polyamide-12 is presented in Fig. 3(a) and (b), before and after binarization respectively.

Using an appropriate image analysis software, one can collect many information for each particle such as its cross-sectional area, long and small axis, coordinates, orientation, etc. as shown on Fig. 3(c) where particles have been individually identified. In the following, these particles are approximated to spheres. An area equivalent diameter, d, is defined for each particle as the diameter of a circle of same cross-sectional area. It is given by:

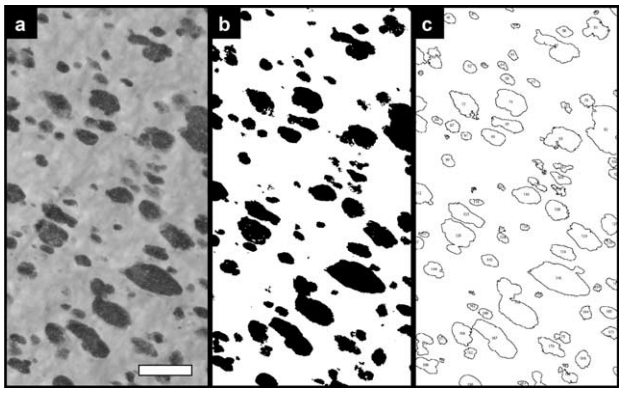

Fig. 3. TEM micrographs of polyamide-12 toughened with 20 wt% of SBM particles (a) initial image (b) binarized image (c) analyzed image where particles are identified, numbered and outlined (scale bar = 2 μm).

$$d = 2\sqrt{\frac{A}{\pi}} \tag{2}$$

where A is the cross-sectional area of the particle measured on the micrograph. Fig. 4 shows the distribution and cumulated density in area equivalent diameter for the system presented in Fig. 3. At this point, the analysis gives 2D measurements which are not corrected from any of the effects described in Section 1.

3.1.2. Cross-section and projection effects

Consider an image obtained from a thin section of a

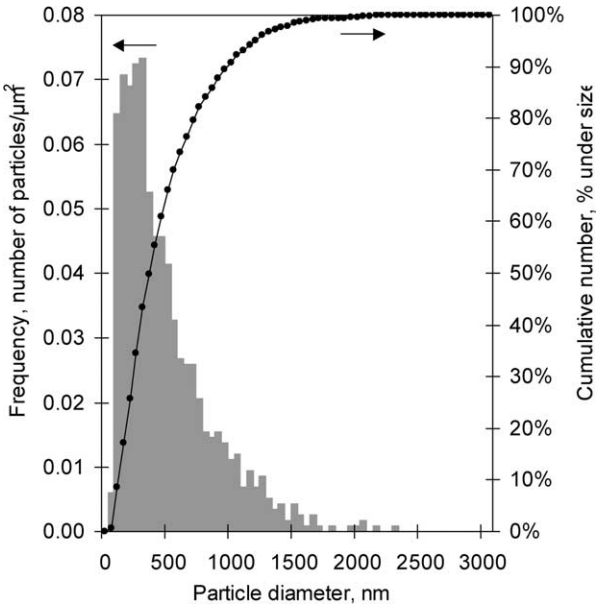

Fig. 4. Two-dimensional distribution in particle diameter for the sample presented in Fig. 3. Diameter is an area equivalent diameter defined by (2).

given thickness, H, as illustrated on Fig. 2. On this image, the apparent diameter, a, of a given particle is not necessarily its real diameter, r, in the bulk. Let $N_A(\cdot)$ be the 2D distribution in apparent diameter and $N_V(\cdot)$ the 3D distribution in real diameter. Practically, $N_A(\cdot)$ and $N_V(\cdot)$ are used in a discrete form. They are divided into the same number of classes, p, of equal class width, Δ. For each class i ($0 \le i \le p$), $N_A(i)$ is the number of particles per unit area which apparent diameter is within the range $[i\Delta, (i+1)\Delta]$. The particle diameter in each class i is represented by its lower limit, $i\Delta$. Similarly, for each class j ($0 \le j \le p$), $N_V(j)$ is the number of particles per unit volume which real diameter is within the range $[j\Delta, (j+1)\Delta[$.

We distinguish the contribution of particles which center is located in or outside the film. For a given class i, $N_A(i)$ is decomposed as follows:

$$N_A(i) = N_A^{in}(i) + N_A^{out}(i) \tag{3}$$

where $N_A^{in}(i)$ and $N_A^{out}(i)$ are the number of particles per unit area belonging to class i and which center is respectively inside or outside the thin section. Particles which center is inside the thin section appear on the image with their real diameter, r, as shown on Fig. 2 for particle 2. Hence, $N_A^{in}(i)$ can be written as:

$$N_A^{in}(i) = HN_V(i) \tag{4}$$

This contribution corresponds to what we described previously as the projection effect.

Particles which center is outside the thin section appear on the image with an apparent diameter, a, smaller than their real diameter r, as shown on Fig. 2 for particles 1 and 3. Hence, $N_A^{out}(i)$ counts the particles which real diameter is greater than $i\Delta$ and which apparent diameter is $i\Delta$. It can be written as the following sum:

$$N_A^{out}(x) = \sum_{j=i}^{p} N_A(i,j) \tag{5}$$

where $N_A(i,j)$ is the number per unit area of particles which have an apparent diameter $i\Delta$ and a real diameter between $j\Delta$ and $(j+1)\Delta$. For each couple (i, j), Fig. 5 shows that the center of such particles is confined into a narrow strip of width dh. There are two such strips corresponding to both faces above and below the film. As a consequence, $N_A(i,j)$ is related to the 3D distribution in real diameter by:

$$N_A(i,j) = N_V(j)2\mathrm{dh} \tag{6}$$

Using Pythagoras theorem, dh can be written as follows:

$$\mathrm{dh} = \frac{\Delta}{2}\left(\sqrt{(j+1)^2 - i^2} - \sqrt{j^2 - i^2}\right) \tag{7}$$

and for each class i,

$$N_A^{out}(i) = \Delta \sum_{j=i}^{p} N_V(j)\left(\sqrt{(j+1)^2 - i^2} - \sqrt{j^2 - i^2}\right) \tag{8}$$

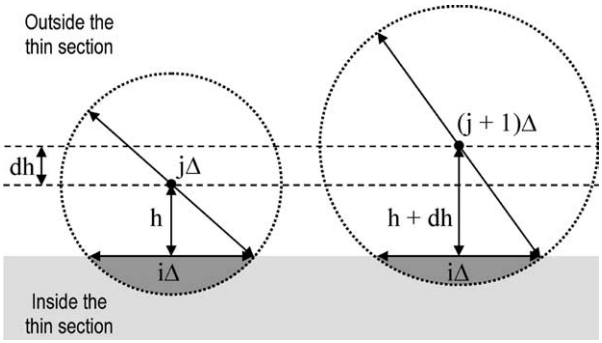

Fig. 5. Correction from the cross-section effect. The idea is to determine the contribution of particles which center is outside the thin section. Consider particles with an apparent diameter $i\Delta$ and a real diameter in the range $[j\Delta, (j+1)\Delta[$. Their center is located within a thin strip of thickness dh.

Substituting (4) and (8) into (3) gives the measured 2D distribution in apparent diameter $N_A(\cdot)$ as a function of the unknown 3D distribution in real diameter $N_V(\cdot)$ as follows:

$$N_A(i) = HN_V(i) + \Delta \sum_{j=i}^{p} N_V(j)\left(\sqrt{(j+1)^2 - i^2} - \sqrt{j^2 - i^2}\right) \tag{9}$$

This last expression can also be written as a tensorial product:

$$\mathbf{N}_A = \mathbf{A}\mathbf{N}_V \tag{10}$$

where $\mathbf{N}_A$ and $\mathbf{N}_V$ are vectors which coordinates are $N_A(i)$ and $N_V(j)$ respectively, and $\mathbf{A}$ is a second order tensor defined by:

$$A_{ij} = 0 \quad \text{if } i > j \tag{11}$$

$$A_{ij} = H\delta_{ij} + \Delta\left(\sqrt{(j+1)^2 - i^2} - \sqrt{j^2 - i^2}\right) \quad \text{if } i \le j \tag{12}$$

For given values of H and Δ, inverting numerically $\mathbf{A}$ gives the 3D distribution in real diameter as a function of the 2D distribution in apparent diameter:

$$\mathbf{N}_V = \mathbf{A}^{-1}\mathbf{N}_A \tag{13}$$

3.1.3. Application to polyamide systems

Two systems of polyamide-12 filled with 10% of small SB(MT) and large SBM particles are analyzed in Figs. 6 and 7 respectively. Corresponding TEM micrographs are given in Figs. 6(a) and 7(a). Figs. 6(b) and 7(b) show the 3D distributions in real diameter reconstructed with three values of section thickness: $H = 0$ nm which ignores the projection effect as if images were obtained by scanning electron microscopy, $H = 60$ and 100 nm which is the typical range of thicknesses obtained by ultramicrotoming. In both systems, reconstructed distributions exhibit negative values for very small particle diameters. This is attributed to

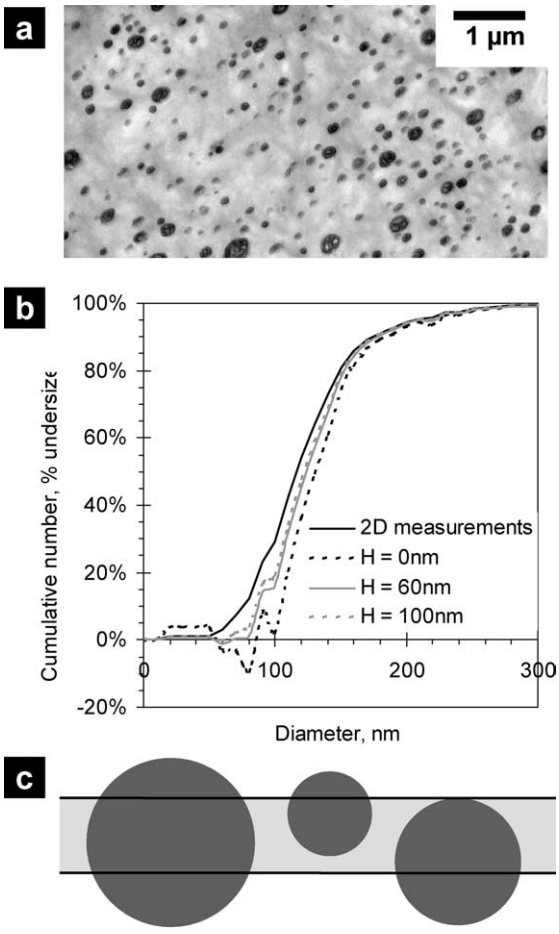

Fig. 6. Analysis of polyamide-12 toughened with 10 wt% of small SB(MT) particles ($d_n \approx 130$ nm) (a) TEM micrograph (b) distribution in particle diameter before and after reconstruction for different values of section thickness ($\Delta = 10$ nm; $H = 0$, 60 and 100 nm) (c) scheme to scale comparing particle size to section thickness.

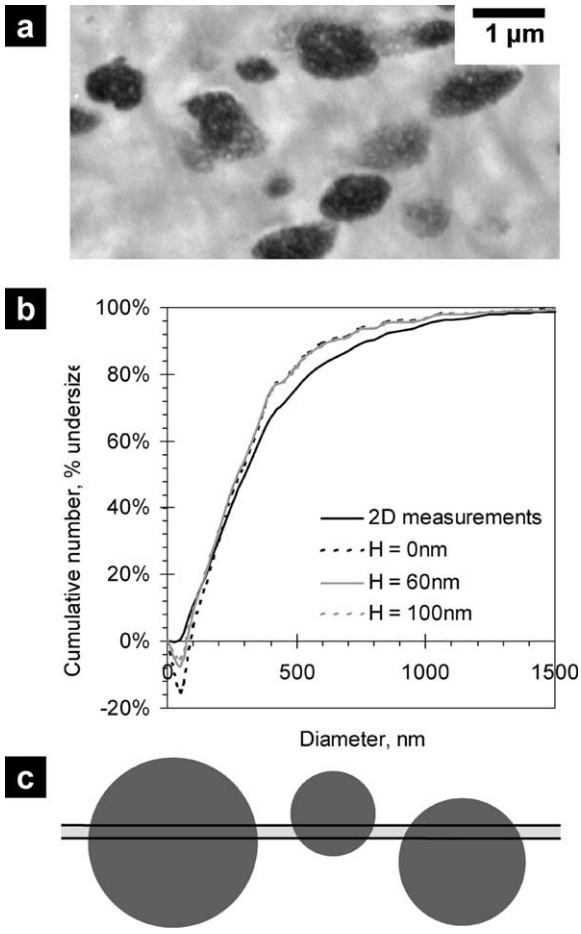

Fig. 7. Analysis of polyamide-12 toughened with 10 wt% of large SBM particles ($d_n \approx 340$ nm) (a) TEM micrograph (b) distribution in particle diameter before and after reconstruction for different values of section thickness ($\Delta = 50$ nm; $H = 0$, 60 and 100 nm) (c) scheme to scale comparing particle size to section thickness.

two factors. First, some of the smallest particles are probably not detected by image analysis [8]. Secondly, the cross-section effect can be overcorrected when the projection effect is not properly considered. Negative values are indeed more pronounced when reconstruction is done assuming an infinitely thin section ($H = 0$ nm).

In the case of small particles, reconstructed distributions given in Fig. 6(b) are significantly shifted towards larger particle sizes. Such shift is expected when correcting data from the cross-section effect which overestimates the fraction of small sizes. However, this correction is less pronounced for the non-zero section thicknesses ($H = 60$ and 100 nm). Here, particle size is comparable to section thickness. As a consequence, many observed particles actually have their center inside the thin section as represented in Fig. 6(c). The magnitude of the projection effect is comparable to that of the cross-section effect so that both corrections must be considered.

In the case of large particles, 3D reconstruction shown in Fig. 7(b) also gives more weight to large particle sizes. However, the section thickness, H, has no or little effect. All three reconstructed distributions for $H = 0$, 60 and 100 nm are very similar. Here, particles are much larger than the section thickness as illustrated in Fig. 7(c). As a result, most particles have their center outside the thin section. Their apparent diameter is smaller than the real one. The projection effect is negligible as compared to the cross-section effect.

To check the quantitative accuracy of the analysis, a good criterion is to back calculate the known volume fraction of filler, Φ, from the reconstructed distribution. Assuming that particles are spherical and taking either the lower ($j\Delta$) or higher, ($(j+1)\Delta$) limit for each class j, the volume fraction should be bounded by the following expression:

$$\sum_{j=0}^{p} N_V(j) \frac{\pi}{6} (j\Delta)^3 \leq \Phi \leq \sum_{j=0}^{p} N_V(j) \frac{\pi}{6} ((j+1)\Delta)^3 \qquad (14)$$

After reconstruction taking a section thickness H of 60 nm, a good agreement is obtained in most cases. For instance, ranges of 9–11% and 12–14% are obtained for

both systems presented in Figs. 6 and 7 respectively, for which the volume fraction is known to be approximately 10%.

3.1.4. Log normal fit

For many particle dispersions [15] and for polymer blends in particular [3], the distribution in particle size often obeys a log-normal distribution. Such statistical law is given by the following density, f_d:

$$f_d(x) = \frac{1}{\sqrt{2\pi}sx}\exp\left[-\frac{(\ln(x)-m)^2}{2s^2}\right] \quad \text{for } x\in]0,+\infty[\tag{15}$$

where s and m are the standard deviation and number average of the distribution in $\ln(x)$ respectively. For PA12/SBM systems, the corrected distributions in particle diameter are very well described by log-normal laws as shown in Fig. 8 for both small and large particles.

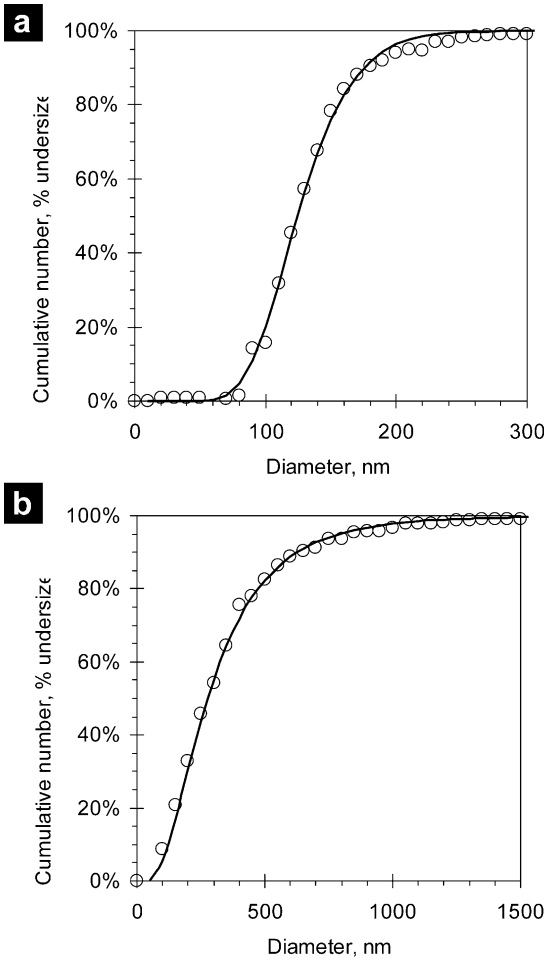

Fig. 8. Log-normal fit of the distributions in particle diameter presented in Figs. 6(a) and 7(b). Open circles correspond to experimental data after correction ($H=60$ nm). Full lines represent the best log-normal fit ((a) $m=4.83$, $s=0.26$, (b) $m=5.59$, $s=0.68$).

3.2. Distribution in ligament thickness

3.2.1. Assumptions

In the following, we estimate the distribution in ligament thickness knowing the particle volume fraction and the distribution in particle size. This method is based on the same assumptions as the initial model of Wu [3]:

1. Particle dispersion is isotropic so that sections along one plane are representative of the whole bulk morphology.
2. Particles are spherical. This is a rather good approximation for the systems presented here. Particles are slightly elongated and their average circularity (ratio of the smallest axis over the larger one) is about 0.6–0.8. In some systems, however, particles can be strongly anisotropic because of their original shape like clays [16] and glass-fibers [17] or because of deformation induced by processing like rubber particles in injection-molded samples [18].
3. Particles are dispersed on a given periodic lattice. Here, we arbitrarily chose a body centered cubic lattice. This is the main restriction of the present method which does not measure the real packing of the particles. As a consequence, the estimated distribution in ligament thickness only results from the distribution in particle size.
4. Particles are randomly dispersed on the lattice regardless of their size meaning that the size of a given particle does not depend on the size of its neighbors. Possible overlap of very large neighbored particles is neglected. The validity of this point will be discussed later.

Within this context, the morphology of a given system is completely described by its filler volume fraction, Φ, and by the density, f_d, of its distribution in particle diameter.

3.2.2. Average ligament thickness

Consider a given system (Φ, f_d) and two neighbored particles A and B of diameter d_A and d_B respectively, as shown on Fig. 9. Ligament thickness, L_{AB}, between A and B is expressed by:

$$L_{AB} = D - \frac{1}{2}(d_A + d_B) \tag{16}$$

where D is the center-to-center distance between particles A

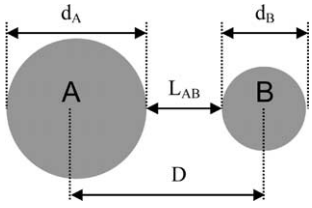

Fig. 9. Assuming a lattice like packing of particles, two nearest neighbored particles A and B are separated by a distance D which is a characteristic length of the chosen lattice. Knowing diameters d_A and d_B of both particles, the ligament thickness, L_{AB}, is expressed by Eq. (16).

and B. The average ligament thickness, L_n, is given by the following expression [9,10]:

$$L_n = d_n\left[C\left(\frac{\pi}{6\Phi}\right)^{1/3} e^{s^2} - 1\right] \tag{17}$$

where C is a constant characterizing the lattice on which particles are supposed to be dispersed (1.00 for cubic, 1.09 for bcc, 1.12 for fcc). Detailed calculations leading to expression (17) are given in the Appendix A.

It is interesting to notice that the average ligament thickness, L_n, is very sensitive to the width of the distribution in particle size through parameter s. Taking $s=0$, one recognizes expression (1) used for particles of same size. In the case of the PA12/SBM systems presented in Fig. 7, the number average diameter, d_n, is 337 nm and filler volume fraction is 10%. If all particles had this same size, the average ligament thickness would be 301 nm. However, in the real system, the standard deviation in particle size is 257 nm ($s=0.68$, $m=5.59$) which leads to a twice larger average ligament thickness of 676 nm.

3.2.3. Distribution in ligament thickness

Let f_L be the density in ligament thickness. In the following, $P[E]$ refers to the probability that event E occurs. Probability that ligament thickness, L_{AB}, between particles A and B is lower than l is given by:

$$P[L_{AB} \le l] = \int_{x=0}^{l} f_L(x)\mathrm{d}x \tag{18}$$

Using (16), this same probability can also be written as follows:

$$P[L_{AB} \le l] = P[d_A + d_B \ge 2(D-l)] \tag{19}$$

$$P[L_{AB} \le l] = \int_{z=2(D-l)}^{+\infty} f_{d+d}(z)\mathrm{d}z \tag{20}$$

where f_{d+d} is the density of variable $Z=d_A+d_B$. Particles are dispersed on the lattice regardless of their size. Hence, d_A and d_B are independent variables which both obey the same statistical law, f_d. Density $f_{d+d}(z)$ is then given by:

$$f_{d+d}(z) = \int_{y=0}^{z} f_d(y)f_d(z-y)\mathrm{d}y \tag{21}$$

As a result, expression (20) becomes:

$$P[L_{AB} \le l] = \int_{z=2(D-l)}^{+\infty}\int_{y=0}^{z} f_d(y)f_d(z-y)\mathrm{d}y\mathrm{d}z \tag{22}$$

Changing variable z into $x=D-z/2$ and considering that f_d equals 0 on $]-\infty, 0]$ gives:

$$P[L_{AB} \le l] = \int_{x=0}^{l}\left[2\int_{y=0}^{2(D-x)} f_d(y)f_d(2D-2x-y)\mathrm{d}y\right]\mathrm{d}x \tag{23}$$

Lastly, comparing (23) with (18) gives the density in ligament thickness f_L as a function of the density in particle diameter f_d:

$$f_L(l) = 2\int_{x=0}^{2(D-l)} f_d(x)f_d(2D-2l-x)\mathrm{d}x \tag{24}$$

For a log-normal distribution in particle size, f_d is given by (14) and f_L is expressed by:

$$f_L(l) = \int_{x=0}^{2(D-l)} \frac{1}{\pi s^2 x(2D-2l-x)} \times \exp\left[-\frac{(\ln(x)-m)^2 + (\ln(2D-2l-x)-m)^2}{2s^2}\right]\mathrm{d}x \tag{25}$$

In Fig. 10, we estimate the distributions in ligament thickness, f_L, for the systems presented in Figs. 6 and 7. Volume fraction of filler, Φ, is about 10%. As it could be expected from (1) with a fixed volume fraction, smaller ligament thicknesses are attained with smaller particles. Not considering possible differences in packing, a clear correlation appears between the distributions in particle size and in ligament thickness. The system with small particles is obtained with reactive fillers of SB(MT). A fast grafting reaction occurs between the amine end groups of the polyamide chains and the reactive T groups introduced in the M block of the SB(MT) chains. As a result, the size of the particles is mostly determined by the reduction of interfacial tension during this chemical grafting between matrix and filler [19]. Such reactive blending produces narrow and rather symmetrical distributions in both particle size and ligament thickness. On the contrary, the system

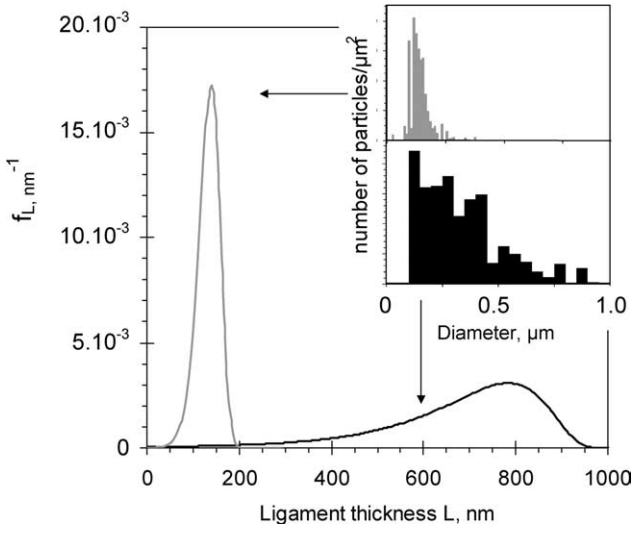

Fig. 10. Distributions in ligament thickness of the system filled with small SB(MT) particles shown in Fig. 6 (grey line) and with large SBM particles shown in Fig. 7 (black line). Histograms in the inset give the corresponding 3D distributions in particle diameter. Calculation is done for a body centered cubic packing of particles ($C=1.09$) and a particle volume fraction, Φ, of 10%. Parameters s and m are determined from the fit given in Fig. 8.

with large particles is obtained with little reactive fillers. Particle size mainly depends on how much the filler is sheared during blending. This results in a broad and asymmetrical distribution in particle size where the fraction of small particles is concentrated in a narrow range between 200 and 500 nm while the fraction of large particles expands on a wide range of sizes up to 2 μm. The corresponding distribution in ligament thickness looks very much similar but reversed. A large fraction of ligaments have their thickness between 0.6 and 1 μm while a smaller population of thin ligaments extends down to thicknesses of about 100 nm.

Besides qualitative considerations, expression (25) also provides additional data to describe the filler dispersions. In particular, it gives an estimate of the standard deviation in ligament thickness, s_L, which can be coupled with the average value, L_n, to better characterize and discriminate the morphologies. For instance, the highly confined system filled with small particles shown in Fig. 6 is characterized by an average ligament thickness, L_n, of about 133 nm and a small standard deviation, s_L, of 24 nm. For the system filled with large particles shown in Fig. 7, L_n is about 684 nm and s_L is 164 nm.

As mentioned above, the present model assumes a lattice-like packing of particles and neglects the possible overlap of particles on the lattice. Fig. 11 shows two extreme cases where these limitations appear. Assuming a lattice-like packing of the particles implies that the ligaments cannot be larger than the characteristic distance between particles, D, given in the Appendix A by (A1). Such approximation may induce a significant error when particles are heterogeneously dispersed. This is the case of the system filled with 5% SBM where particle dispersion is rather heterogeneous as shown by the TEM micrograph on top of Fig. 11. On the image, some ligaments are clearly larger than the lattice size, D, which is about 1470 nm. However, for higher filler concentrations, dispersions are more homogeneous and there is no clear discrepancy between estimations and TEM observations.

The present model also supposes that particles are randomly dispersed on a given lattice regardless of their size. As a consequence, two large particles could stand next to each other on the lattice even though the sum of their radius is greater than the characteristic distance between neighbored particles, D. This leads to a contradiction where the two particles overlap each other. By definition, the value $f_L(0)$ gives an estimation of the number of these overlaps. In most cases, the characteristic distance, D, is large enough compared to the largest particle sizes and overlaps can reasonably be neglected. However, as the filler concentration increases, the characteristic distance, D, decreases and the contribution of overlaps becomes significant as shown by the inset in Fig. 11. In the system filled with 30% SBM particles, the importance of overlaps could be guessed from the TEM micrograph where the size of the largest particles looks comparable or even greater than the characteristic center-to-center distance.

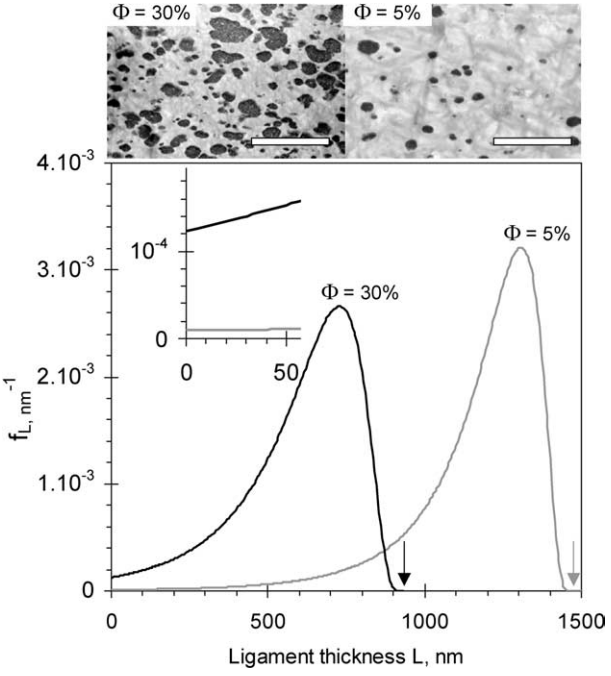

Fig. 11. Distributions in ligament thickness in polyamide-12 filled with 5% (gray line) and 30% (black line) of SBM particles. TEM micrographs are shown at the top (scale bar = 5 μm). Arrows on the graph indicate the value of the characteristic lattice size, D, obtained from (A1). Close-up in the top left corner shows the effect of particle overlap.

4. Conclusion

Analysis of electron microscopy images is a useful tool to characterize particle dispersions in polymer blends. To obtain quantitative results, it is necessary to reconstruct true 3D data from 2D measurements. In most cases, analysis is performed on scanning electron micrographs which show cross-sections of the bulk morphology. In this paper, we have considered the use of transmission electron microscopy which, unlike scanning electron microscopy, gives a 2D projection of a thin section. In order to reconstruct the true 3D distribution in particle size, we apply a Schwartz-Saltikov algorithm which corrects both the cross-section and the projection effects. Practical examples on toughened systems of polyamide-12 confirms that the effect of section thickness becomes significant when particle size is comparable to section thickness. By extending the method of Wu, it is possible to estimate the whole distribution in ligament thickness and in particular its width. This calculation provides a simple way to describe the particle dispersion but assumes that particles are randomly dispersed on a regular lattice. Practical cases on toughened polyamide-12 show that this rather strong assumption can be a limitation in extreme cases when particle dispersion is heterogeneous or when the size of the

largest particles is comparable to the characteristic center-to-center distance.

Acknowledgements

The authors thank P. Coupard (ARKEMA) for TEM micrographs of PA12/SB(MT) systems. Financial support from ARKEMA, CNRS and ESPCI is also gratefully acknowledged. The authors declare that they have no competing financial interests.

Appendix A. Average ligament thickness

We only consider nearest neighbors so that for a given lattice, center-to-center distance, D, is a characteristic length given by:

$$D = C\left(\frac{1}{N}\right)^{1/3} \tag{A1}$$

where C is a constant determined by the nature of the lattice (1.00 for cubic, 1.09 for bcc, 1.12 for fcc). N is the total number of particles per unit volume. It is related to Φ and f_d by the following expression:

$$\Phi = \int_0^\infty \frac{4}{3}\pi\left(\frac{x}{2}\right)^3 N f_d(x)\mathrm{d}x = \frac{\pi}{6}NM_3 \tag{A2}$$

where M_3 is the third moment of f_d.

Particles are assumed to be dispersed on the lattice regardless of their size. In other words, the diameters of neighbored particles are independent variables so that using (16), the number average ligament thickness, L_n, is simply expressed by:

$$L_n = D - d_n \tag{A3}$$

Substituting (A1) and (A2) in (A3), L_n can be written in terms of particle concentration, Φ, and distribution in particle size, f_d:

$$L_n = C\left(\frac{\pi M_3}{6\Phi}\right)^{1/3} - d_n \tag{A4}$$

For a log-normal distribution in particle size, f_d is expressed by (14) and d_n and M_3 are given by:

$$d_n = e^{m+(1/2)s^2} \tag{A5}$$

$$M_3 = e^{3m+(9/2)s^2} \tag{A6}$$

Finally, the average ligament thickness, L_n, is estimated by substituting (A5) and (A6) in (A4):

$$L_n = d_n\left[C\left(\frac{\pi}{6\Phi}\right)^{1/3} e^{s^2} - 1\right] \tag{A7}$$

References

[1] Paul DR, Barlow JW. Polymer blends (or alloys). J Macromol Sci-Part C 1980;18:109–68.
[2] Ruzette A-V, Leibler L. Block copolymers in tomorrow's plastics. Nat Mater 2005;4:19–30.
[3] Wu S. Phase structure and adhesion in polymer blends: a criterion for rubber toughening. Polymer 1985;26:1855–63.
[4] Kayano Y, Keskkula H, Paul DR. Evaluation of the fracture behaviour of nylon-6/SEBS-*g*-MA blends. Polymer 1997;38:1885–902.
[5] Schrauwen BAG, Govaert LE, Peters GWM, Meijer HEH. The influence of flow-induced crystallization on the impact toughness of high-density polyethylene. Macromol Symp 2002;185:89–102.
[6] Corté L, Beaume F, Leibler L. Crystalline organization and toughening: example of polyamide-12. Polymer 2005;46:2748–57.
[7] Saltikov SA. The determination of the size distribution of particles in an opaque material from a measurement of the size distribution of their sections. Proceedings of the second international congress for stereology 1967. p. 163–73.
[8] Giumelli AK, Militzer M, Hawbolt EB. Analysis of the austenite grain size distribution in plain carbon steels. ISIJ Int 1999;39:271–80.
[9] Wu S. A generalized criterion for rubber toughening: the critical ligament thickness. J Appl Polym Sci 1988;35:549–61.
[10] Bartczak Z, Argon AS, Cohen RE, Weinberg M. Toughness mechanism in semi-crystalline polymer blends: I. High-density polyethylene toughened with rubbers. Polymer 1999;40:2331–46.
[11] Sigalov GM, Ibuki J, Chiba T, Inoue T. Method of effective ellipses for digital image analysis of size, shape, orientation, and interparticle distances in polymer blends: application to a study of polyamide 6/polysulfone reactive blending. Macromolecules 1997;30:7759–67.
[12] Rebizant V, Venet A-S, Tournilhac F, Girard-Reydet E, Navarro C, Pascault J-P, et al. Chemistry and mechanical properties of epoxy-based thermosets reinforced by reactive and non-reactive SBMX block copolymers. Macromolecules 2004;37:8017–27.
[13] Rebizant V. PhD Thesis, Université Pierre et Marie Curie, Paris; 2003.
[14] ImageJ software: available at http://rsb.info.nih.gov/ij/.
[15] Limpert E, Stahel WA, Abbt M. Log-normal distributions across the sciences: keys and clues. BioScience 2001;51:341–52.
[16] Sinha Ray S, Okamoto M. Polymer/layered silicate nanocomposites: a review from preparation to processing. Prog Polym Sci 2003;28:1539–641.
[17] Clarke AR, Archenhold G, Davidson NC. A novel technique for determining the 3D spatial distribution of glass fibers in polymer composites. Compos Sci Technol 1995;55:75–91.
[18] Moffit M, Rharbi Y, Chen W, Tong JD, Winnik MA, Thurman DW, et al. Stratified morphology of a propylene/elastomer blend following channel flow. J Polym Sci-Part B 2001;40:2842–59.
[19] Groeninckx G, Harrats C, Thomas S. In: Scott W, Hu G-H, editors. Reactive polymer blending baker, 2001. p. 44–79.